

# Strength-Based Topology Optimization for Anisotropic Parts

Amir M. Mirzendehtdel, Behzad Rankouhi, Krishnan Suresh

*Department of Mechanical Engineering, University of Wisconsin-Madison, WI 53706, United States*

---

## ABSTRACT

Additive manufacturing (AM) is emerging as a promising technology to fabricate cost-effective, customized functional parts. Designing such functional, i.e., load bearing, parts can be challenging and time consuming where the goal is to balance performance and material usage. Topology optimization (TO) is a powerful design method which can complement AM by automating the design process. However, for TO to be a useful methodology, the underlying mathematical model must be carefully constructed. Specifically, it is well established that parts fabricated through some AM technologies, such as fused deposition modeling (FDM), exhibit behavioral anisotropy. This induced anisotropy can have a negative impact on functionality of the part, and must be considered. To the best of our knowledge, a robust TO method to handle anisotropy has not been proposed. In the present work, a strength-based topology optimization method for structures with anisotropic materials is presented. More specifically, we propose a new topological sensitivity formulation based on strength ratio of non-homogeneous failure criteria, such as Tsai-Wu. Implementation details are discussed throughout the paper, and the effectiveness of the proposed method is demonstrated through numerical and experimental tests.

**Keywords** *Topology Optimization, Additive Manufacturing, Level-set method, Pareto tracing, Anisotropic Materials, Strength, Failure Index, Tsai-Wu.*

---

## 1. Introduction

Additive manufacturing (AM) is becoming increasingly popular for fabricating prototypes, and customized production parts. Furthermore, AM is well-suited for small-batch production and on-spot fabrication where transporting built parts is expensive or even impossible. Currently, the most accessible AM technology is Fused Deposition modeling (FDM) where material is extruded from a nozzle, and the part is built layer by layer. FDM is fairly robust with respect to build scale and material [1]. This, along with other advantages such as ease of use, portability, affordability, and safety make FDM very promising in producing functional parts in applications such as:

- a) Large-scale printing (cars and houses) [1], [2]
- b) Biomedical customized parts [3]
- c) Electronics-embedded designs, e.g. Figure 1 [4]
- d) Printing in hostile places, e.g. space missions [5]



**Figure 1:** FDM printed functional quadcopter. Printed via Voxel8 with embedded electronics and endures structural loading [4].

---

Topology optimization (TO) [6]–[8] is used at early stages of design to automatically reduce weight and material usage while

satisfying constraints on performance. AM and TO complement each other in that organic and complex designs generated through TO can be manufactured through AM technologies. On the other hand, the cost of AM parts increase significantly with material usage. Thus optimizing designs can be crucial in saving material usage, build time, and post-process time [9].

However, there are certain challenges in TO for AM which need to be addressed before the two fields can be seamlessly integrated. Material anisotropy and weakness along build direction, especially in FDM, is an important consideration. This issue becomes more critical when the part is functional and has to satisfy strength-related constraint. There are mainly two types of anisotropy, namely 1) intrinsic e.g. composites and 2) process induced. Intrinsic anisotropy is often favorable since it can provide more freedom through intentionally creating directional preference in behavior. On the other hand, process-induced anisotropy is the result of process limitations and is often unfavorable. In this paper, we focus on addressing material anisotropy induced throughout FDM process due to lack of interlayer fusion as illustrated in Figure 2. Note that anisotropy in FDM could manifests itself in two ways: 1) anisotropic constitutive properties relating stress and strain, and 2) directional strengths. However, current experimental results suggest that in some cases (see section 4), printed parts exhibit isotropic constitutive properties [10]. The focus of this paper is on strength anisotropy.

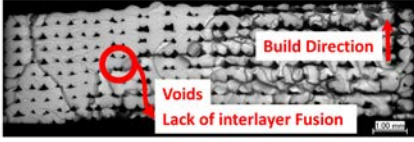


**Figure 2:** Micro fractographs of 3D printed samples using FDM. Different raster orientations plays and important role in mechanical behavior of parts [11].

In section 2 we will review literature on stress-constrained TO for both isotropic (2.1) and anisotropic (2.2) materials. In section 3 we will describe the proposed method and define the strength-based TO problem (3.1), perform sensitivity analysis (3.2 and 3.3), and present the proposed optimization algorithm (3.4). Finally, in section 4 we demonstrate the effectiveness of the proposed method through numerical and experimental results.

## 2. Literature Review

A typical TO problem can be posed as follows: given an initial design space  $D$ , we want to find an optimal topology that minimizes an objective while satisfying several constraints,

$$\begin{aligned}
 & \underset{\Omega \subset D}{\text{minimize}} && f(\Omega, \mathbf{u}) \\
 & g_i \leq 0 && i = 1, \dots, N \\
 & \text{subject to} && \\
 & \mathbf{K}\mathbf{u} = \mathbf{f} && 
 \end{aligned} \tag{1}$$

where:

- $D$ : Design space
- $\Omega$ : Optimized design
- $f$ : Objective
- $g_i$ : Constraints: volume, displacement,...
- $\mathbf{u}$ : Displacement vector
- $\mathbf{K}$ : Stiffness matrix
- $\mathbf{f}$ : External force vector

Perhaps the most common objective is compliance for which the TO is fairly straight forward [12]. However, in order to design functional parts, we must consider minimizing stress where sensitivity analysis can be quite challenging due to locality and non-linearity of stress with respect to design variables. The former results in a huge number of constraints for even moderately complex problems, and the latter affects the convergence of the optimization process. Due to these challenges, there have been fewer attempts focusing on strength optimization compared to stiffness, and even less using anisotropic material properties.

### 2.1 Strength Optimization for Isotropic Materials

There are numerous failure criteria that have been developed for isotropic materials over the years; the most common ones are based on maximum principal stress by Rankine, maximum

principal strain by St. Venant, total strain energy by Beltrami, maximum shear stress by Tresca, and octahedral shear stress by von Mises. Among these, Rankine is best suited for brittle materials and vonMises agrees best with ductile materials [13].

Earlier attempts towards producing strength-based optimum structural designs were mainly focused on shape optimization [14], [15] and topology optimization of trusses [16]. It was believed by many [17]–[20] that the optimal design might be an isolated or singular point in the design space. For instance for truss optimization, as was shown by Kirsch [19], a singularity phenomenon occurs as the cross-section of a bar reaches its lower bound of zero. This, as explained later by Cheng and Jiang [21], was due to discontinuity of the stress function and the fact that the constraint function of the optimization problem becomes undefined. Cheng and Guo [22] proposed an  $\varepsilon$ -relaxation method as a solution to this issue, where the singular optimum design was eliminated from the design space; consequently, sizing and topology optimization could be unified in a single framework (also see [23], [24]).

Since the development of homogenization method by Bendsøe and Kikuchi [25] and Solid Isotropic Material with Penalization (SIMP) method by Bendsøe [26], many different strategies have been proposed for stress-based TO. For instance, Xie and Steven [27] proposed an evolutionary method, in which elements with lower von-Mises stress are gradually rejected. This approach could lead to sub-optimal designs, due to locality nature of stress [28].

Perhaps the most popular TO method is SIMP, where a pseudo-density variable  $\rho$  ( $0 \leq \rho \leq 1$ ) is used to describe material distribution. Yang and Chen [29] used a global stress measure such as Kreisselmeier-Steinhauser or Park-Kikuchi as the objective function. In particular, their objective was a weighted average of compliance and the p-norm of a stress measure.

It is well-known that as  $\rho$  approaches 0, the stress values can become singular, which results in the same type of singularity phenomenon discussed above. In order to overcome this problem, Duysinx and Bendsøe [30], proposed an  $\varepsilon$ -relaxation scheme for SIMP. Bruggi and Venini [31] and Bruggi [32] proposed an alternative qp-approach to remedy the singularity problem, which required less computational effort. Le et al. [33] proposed a formulation based on normalized stress p-norm and a density filter to control length scale. París et al. [34], proposed a TO method considering local and global stress constraints. They later extended their work in [35] by developing block aggregated approach, where one stress constraint was assigned to a group of elements. As was shown in [30], TO with a global stress constraint can be too coarse and might yield results similar to those of stiffness optimization. The clustered approach can avoid stress concentrations and give better designs while not being too

expensive. Along these lines, in [36], the number of stress constraints are reduced by clustering several stress evaluation points into groups.

The level-set (LS) method [7], [37], [38] is another popular approach for TO, where the boundaries of the design are defined as zero level sets of a scalar level-set function. In the conventional form, the Hamilton-Jacobi partial differential equations have to be solved to update design boundaries.

In [39], Miegroet and Duysinx proposed a LS method to minimize the stress concentration of 2D fillets. The approach uses X-FEM, which enriches classical finite element method (FEM) with several discontinuous shape functions. Svanberg and Werme [40], presented two sequential integer programming methods, where a sequence of linear or quadratic sub-problems with decreasing mesh sizes are solved and on the fine level. A LS method was proposed in [41] to minimize stress of designs in 2D and 3D, where the Hamilton-Jacobi transport equation governs the evolution of the LS.

In this framework no new holes can be introduced into the design and only pre-existing features can merge together, making the optimized design heavily dependent on the initial design. To overcome this challenge, the topological sensitivity field based level-set was introduced in [42]–[44]. A rigorous mathematical formulation was later provided by Novotny et al. [12]. In essence, topological sensitivity is the first-order change in objective functional if a small hypothetical hole is introduced in the domain.

Amstutz and Novotny [45] developed the topological derivatives for a stress-based objective function consisted of compliance, volume, and the p-norm of von Mises stress. Xia et al. [46] introduced a global measure of stress based on von Mises stress and Heaviside function. The sensitivity analysis was then carried out by solving an adjoint problem [47]. Finally, the optimization problem was solved using LS method. Suresh and Takaloozadeh [48] proposed a LS-based Pareto-front tracing algorithm. The proposed LS method used p-norm of von-Mises stress as the global measure to solve the optimization problem. Cai et al. [49] integrated LS function and B-spline finite cell method to improve the accuracy of stress and sensitivity evaluation. A combination of LS and augmented Lagrangian was introduced in [50], where stress constraints were assigned to a neighborhood of nodes to capture local effects while remaining continuous. Cai and Zhang [51] recently proposed an LS method for free-form design domains using Boolean operations. The method also exploits a dynamic aggregation technique to reduce the number of local stress constraints.

Although the topological sensitivity is a well-established concept, it is mainly used when underlying material properties are isotropic, i.e. when closed-form gradients can be efficiently evaluated. Although there have been valuable theoretical contributions towards computing anisotropic topological

sensitivities, they have not yet been employed in an optimization algorithm successfully. Schneider and Andr a [52] proposed a closed-form solution for topological sensitivity for materials with anisotropic constitutive properties, which involves considering ellipsoidal inclusions and computing Eshelby’s tensor. Delgado and Bonnet [53] also proposed an asymptotic topological sensitivity for anisotropic stress functionals. In both cases the mathematical derivations are extremely complex and are yet to be exploited in an efficient optimization framework.

In sub-section 2.2 and section 3, we will discuss an alternative sensitivity analysis based on generalized failure criteria and discrete element sensitivity.

## 2.2 Strength Optimization for Anisotropic Materials

A generalization of von Mises criterion was introduced by Hill [54] for orthotropic materials. Later, Azzi and Tsai [55] presented another failure criterion, generally known as Tsai-Hill criterion that simplified Hill’s criterion for unidirectional composites. However, Hill and Tsai-Hill criteria did not take into consideration the behavioral differences between tension and compression. This limitation was overcome by Hoffman [56] by including additional linear terms. Encompassing these ideas, Tsai and Wu [57] proposed a general criterion for anisotropic materials in the following tensor form,

$$\mathcal{F} = \sum_{j=1}^6 \sum_{i=1}^6 C_{ij} \sigma_i \sigma_j + \sum_{i=1}^6 C_i \sigma_i \leq 1 \quad (3)$$

where

$$\begin{aligned} \sigma_1 &= \sigma_{11} & \sigma_2 &= \sigma_{22} & \sigma_3 &= \sigma_{33} \\ \sigma_4 &= \sigma_{23} & \sigma_5 &= \sigma_{31} & \sigma_6 &= \sigma_{12} \end{aligned} \quad (4)$$

Often the coupling between shear terms can be neglected [58]; Equation (3) can then be reduced to that of Equation (5),

$$\mathcal{F} = \mathcal{A} + \mathcal{B} \leq 1 \quad (5)$$

where

$$\begin{aligned} \mathcal{A} &= 2C_{12} \sigma_1 \sigma_2 + 2C_{13} \sigma_1 \sigma_3 + 2C_{23} \sigma_2 \sigma_3 + \\ &C_{11} \sigma_1^2 + C_{22} \sigma_2^2 + C_{33} \sigma_3^2 + C_{44} \sigma_{23}^2 + C_{55} \sigma_{31}^2 + C_{66} \sigma_{12}^2 \\ \mathcal{B} &= C_1 \sigma_1 + C_2 \sigma_2 + C_3 \sigma_3 \end{aligned} \quad (6)$$

The coefficients are given by:

$$\begin{aligned}
C_1 &= \frac{1}{X_t} - \frac{1}{X_c}, C_2 = \frac{1}{Y_t} - \frac{1}{Y_c}, C_3 = \frac{1}{Z_t} - \frac{1}{Z_c} \\
C_{12} &= \frac{-1}{2\sqrt{X_t X_c Y_t Y_c}}, C_{13} = \frac{-1}{2\sqrt{X_t X_c Z_t Z_c}}, C_{23} = \frac{-1}{2\sqrt{Y_t Y_c Z_t Z_c}} \\
C_{11} &= \frac{1}{X_t X_c}, C_{22} = \frac{1}{Y_t Y_c}, C_{33} = \frac{1}{Z_t Z_c} \\
C_{44} &= \frac{1}{S_{23}^2}, C_{55} = \frac{1}{S_{31}^2}, C_{66} = \frac{1}{S_{12}^2}
\end{aligned} \tag{7}$$

where  $X_t, Y_t, Z_t$  are tensile strengths,  $X_c, Y_c, Z_c$  are compressive strengths, and  $S_{23}, S_{31}, S_{12}$  are shear strengths.

Tsai-Wu criterion is widely used due to its 1) invariance with respect to basis, 2) symmetry, and 3) generality.

It has also been used in the context of optimization. In order to optimize fiber orientations in composite laminates, Groenwold and Haftka [59] proposed a sensitivity analysis based on the Tsai-Wu criterion. However, it was shown in [59] that using a non-homogeneous failure index such as Tsai-Wu as the objective function would be load-dependent (sensitive to load intensity) and may result in counter-intuitive designs. To overcome these limitations, they proposed using the safety factor or strength-ratio discussed in the next section.

## 2.3 Maximizing Anisotropic Strength

Consider the failure index in Equation (5):

$$\mathcal{A} + \mathcal{B} - 1 \leq 0 \tag{8}$$

Observe that this applies at each point within the domain, i.e., in practice, at each element within the mesh. For reasons, discussed above, it was proposed in [59] that one should consider the safety factor (also referred to as strength ratio), defined as the positive solution to the quadratic Equation (9),

$$\mathcal{A}s_e^2 + \mathcal{B}s_e - 1 = 0 \tag{9}$$

i.e.,

$$s_e = \frac{-\mathcal{B} + \sqrt{\mathcal{B}^2 + 4\mathcal{A}}}{2\mathcal{A}} \tag{10}$$

The goal therefore will be to maximize the safety factor at each element. Alternately, the goal is to minimize the failure index at each element, defined as:

$$\gamma_e = \frac{1}{s_e} \tag{11}$$

One can aggregate these failure indices via the p-norm ([33], [46], [48], [60]) into a single global failure index:

$$\gamma = \|\gamma_e\|_p = \left( \sum_e (\gamma_e)^p \right)^{1/p} \tag{12}$$

In this paper we will devise a TO framework based on the objective in Equation (12).

## 3. Proposed Strategy

In this section, we will discuss the optimization problem (3.1), proposed sensitivity analysis (3.3), and optimization algorithm (3.4).

### 3.1 Optimization Problem

Based on the discussion in the previous section, the TO problem considered in this paper is:

$$\begin{aligned}
&\text{minimize } \gamma \\
&\quad \Omega = D \\
&J \leq \bar{J} \\
&\text{subject to} \\
&\mathbf{Ku} = \mathbf{f}
\end{aligned} \tag{13}$$

where  $\bar{J}$  is the (user defined) allowable compliance at the target volume fraction. Observe that (1) a compliance constraint is essential to avoid pathological conditions [61], (2) the failure criteria of Equation (5) is not explicitly imposed since it is absorbed into the objective; however, this can be easily imposed as an additional check.

### 3.2 Sensitivity Analysis

To solve the TO problem of Equation (13) one must first compute the sensitivity of the objective and compliance constraint.

To this end, let us consider the corresponding Lagrangian [62]:

$$L(\Omega, \mathbf{u}; \lambda_j) = \gamma - \lambda_j (J - \bar{J}) \tag{14}$$

where  $\lambda_j$  is the Lagrange multiplier associated with the compliance constraint.

Recall that the topological sensitivity at a point  $p$  for any quantity of interest  $\varphi$  is defined as [48]:

$$\mathcal{T}_\varphi(p) \equiv \lim_{r \rightarrow 0} \frac{\varphi(r; p) - \varphi_0}{\pi r^2} \tag{15}$$

One can apply this concept to the Lagrangian [63] as follows:

$$\mathcal{T}_L = \mathcal{T}_\gamma - \lambda_j \mathcal{T}_J \tag{16}$$

While closed-form expressions for the topological sensitivity of the compliance exist [64], a closed-form expression for the failure index does not exist. We will therefore consider an alternate ‘discrete element sensitivity’, defined as the change in any quantity of interest when a single element ‘ $e$ ’ is deleted from the mesh:

$$\mathcal{D}_\varphi(e) \equiv \frac{\varphi(\Omega - e) - \varphi(\Omega)}{|e|} \quad (17)$$

where  $|e|$  is area of the element.

Similar to Equation (16), the discrete sensitivity can be applied to the Lagrangian resulting in:

$$\mathcal{D}_L = \mathcal{D}_\gamma - \lambda_j \mathcal{D}_j \quad (18)$$

For compliance, one can show that the discrete sensitivity is given by (see [65]):

$$\mathcal{D}_j = \mathbf{u}_e^T \mathbf{K}_e \mathbf{u}_e \quad (19)$$

Figure 3 compares discrete sensitivity against the topological sensitivity for compliance for the L-bracket. Observe that the two fields are quite similar since they essentially capture the first order change in compliance when material is removed.

In the next section, we focus on computing the discrete sensitivity  $\mathcal{D}_\gamma$  for anisotropic strength.

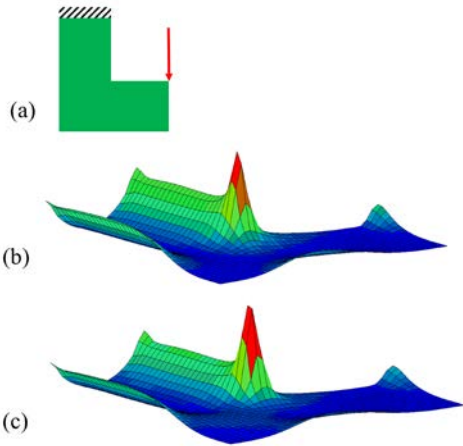


**Figure 3:** a) L-bracket geometry, b) topological sensitivity  $\mathcal{T}_j$  and c) discrete element sensitivity  $\mathcal{D}_j$  [65].

### 3.3 Sensitivity Analysis of Strength

To compute  $\mathcal{D}_\gamma$  we use the strategy proposed in [48]. Specifically, using the chain rule we have:

$$\mathcal{D}_\gamma = (\nabla_{\mathbf{u}} \gamma)^T \mathcal{D}(\mathbf{u}) \quad (20)$$

where  $\mathcal{D}(\mathbf{u})$  is the change in displacement field due to the deletion of an element. One can show that this is given by [65]:

$$\mathcal{D}(\mathbf{u}) = (\mathbf{K}^{-1} \Delta \mathbf{K}_e) \mathbf{u} \quad (21)$$

where  $\Delta \mathbf{K}_e$  is the corresponding element stiffness matrix (mapped to the global indices). Substituting Equation (21) in Equation (20) leads to:

$$\mathcal{D}_\gamma = (\nabla_{\mathbf{u}} \gamma)^T (\mathbf{K}^{-1} \Delta \mathbf{K}_e) \mathbf{u} \quad (22)$$

Further, define the vector

$$\mathbf{g} \equiv \nabla_{\mathbf{u}} \gamma \quad (23)$$

In the Appendix of this paper, we show that a computable expression can be derived for  $\mathbf{g}$ , i.e.,  $\mathbf{g}$  can be computed as a post-processing step. Thus, we have:

$$\mathcal{D}_\gamma = \mathbf{g}^T \mathbf{K}^{-1} (\Delta \mathbf{K}_e) \mathbf{u} \quad (24)$$

Now define and solve the adjoint problem:

$$\mathbf{K} \boldsymbol{\mu} = \mathbf{g}^T \quad (25)$$

Thus:

$$\mathcal{D}_\gamma = \boldsymbol{\mu}^T (\Delta \mathbf{K}_e) \mathbf{u} \quad (26)$$

This can be simplified to an element-wise construction [65],

$$\mathcal{D}_\gamma = \boldsymbol{\mu}_e^T \mathbf{K}_e \mathbf{u}_e \quad (27)$$

Thus, the element-wise discrete sensitivity of the Lagrangian is given by Equation (18).

### 3.4 Algorithm

Once the discrete sensitivity fields are computed, we can use the algorithm discussed in this section to solve the TO problem of Equation (13).

The Lagrange multiplier in Equation (18) can be dynamically computed through the augmented Lagrangian method described, for example in [62]. Here, we will use an alternate (and equivalent) updating scheme proposed in [48] where the Lagrangians are interpreted as weights:

$$\mathcal{D}_L = w \mathcal{D}_\gamma + (1-w) \mathcal{D}_j \quad (28)$$

$$0 \leq w \leq 1$$

Similar to the augmented Lagrangian method, the weights are dynamically updated as follows. To begin with, the weight  $w$  is set to 1, i.e., the topology is entirely driven by the objective (to minimize anisotropic failure).

The resulting sensitivity field is directly interpreted as a level-set, leading to the PareTO (Pareto-tracing Topology Optimization) discussed in [8], [48], [65], [66]. Using fixed-point iteration, the a small-step (that is dynamically modified) is taken along the Pareto curve. If the compliance constraint is violated the weight is reduced by a factor  $\eta$  (similar to the augmented Lagrangian method). The overall algorithm is illustrated in Figure 4 and the details are as follows:

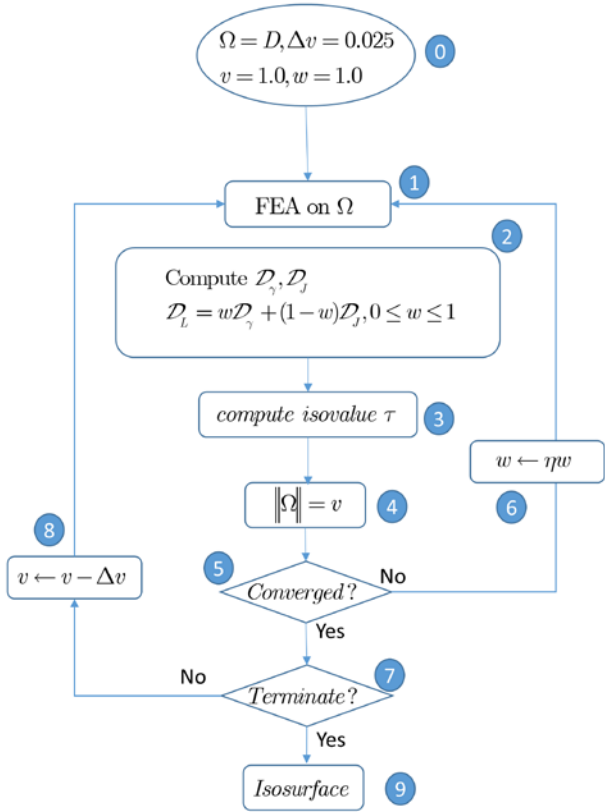


Figure 4: The proposed algorithm

0. Initialization: we start with an initial design space  $D$  where current volume fraction  $v$  is set to 1.0, and at every TO step  $v$  is reduced by  $\Delta v$  (typically 0.025). The weighting factor  $w$  in Equation (28) is initialized to 1.0.
1. Solve the finite element problem on the current topology  $\Omega$ .
2. Compute discrete element sensitivity  $\mathcal{D}_L$  via Equations (19) and (27).
3. Compute level-set cutoff isovalue  $\tau$  using fixed-point iteration.
4. Update topology.
5. Check if current  $\tau$  has converged,
6. If not, reduce weight  $w$  by a factor  $0 < \eta < 1$  (typically  $\eta = 0.9$ ) and go to step 1.
7. Check if desired volume has been reached or any of the constraints are violated.
8. If not, reduce volume by  $\Delta v$  and repeat from step 1.
9. If yes, generate isosurface of the final design.

#### 4. Experiments and Validations

In this section, we demonstrate the effectiveness of proposed method through numerical and experimental examples. Due to complexity of FDM-induced anisotropy, the experiments are conducted under the following assumptions.

**Constitutive Properties.** As discussed in Section 1, the (stress-strain) constitutive properties of FDM-printed parts are affected by numerous parameters. Here, we use the constitutive properties of ABS recently reported by Riddick et al. [10] considering  $\pm 45^\circ$  raster orientation. It was reported in [10] that the primary constitutive properties namely, the Young’s modulus and Poisson ratio were the same along both the raster orientation (S1) and build direction (V1), specifically,  $E = 2.76 \text{ GPa}$  and  $\nu = 0.38$ . Thus, it exhibits isotropic constitutive properties (but not isotropic strength).

**Anisotropic Strengths.** For the Tsai-Wu failure criteria, 9 strength components (3 tensile, 3 compressive, and 3 shear) must be evaluated. We will use strength values reported in relevant literature (see Table 1). The three compressive strengths and three shear strengths are approximated according to the results reported in Ahn et al. [67] and Ahn et al. [68]. The three tensile strengths are assumed to be consistent with values reported in [10] considering  $\pm 45^\circ$  raster orientation (S1 and V1).

Note that these simplifications are merely a convenience; the topology optimization framework proposed in the paper can handle alternate models.

Table 1: Material strengths

Material	Xc (MPa)	Yc (MPa)	Zc (MPa)	Xt (MPa)	Yt (MPa)	Zt (MPa)	Syz (MPa)	Szx (MPa)	Sxy (MPa)
ABS (FDM)	38	38	35	29.62	29.62	19.80	10	10	10

**Interaction Coefficients.** The three in-plane interaction terms  $C_{12}$ ,  $C_{13}$ , and  $C_{23}$  are expressed in terms of bi-axial strengths and are often not readily available, especially in 3D. The approximate values for these coefficients are consistent with [59] (see Equation (7)). More careful examinations on the effects of geometry and print parameters on these parameters and subsequently Tsai-Wu criterion is required.

For computing p-norm  $p = 6$ . All numerical experiments are performed on an off-the-shelf desktop with an Intel Core i7 @3.00GHz CPU and 16 GB memory.

#### 4.1 Stiffness Versus Strength

In this example, we demonstrate why maximizing strength might yield a more suitable design than maximizing stiffness. To this end, let us consider the simple tensile test illustrated in Figure 5 where the geometry is a cube with dimensions of  $5 \text{ cm} \times 5 \text{ cm} \times 5 \text{ cm}$ . A unit force is applied at the center of top surface while four bottom corners are fixed. Bottom surface is retained for experimental purposes. The goal is to find the strongest design while 80% of material is removed. The domain is discretized into 50,000 hexahedral elements.

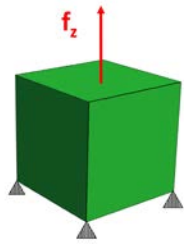


**Figure 5:** Tensile stool. Geometry and loading.

In order to compare the optimized design with respect to stiffness and strength, we first solve Equation (1) where the objective functional  $f$  is compliance. The optimized topology at 0.2 weight fraction is shown in Figure 6a. Next, we solve the proposed optimization problem of Equation (13), where weakness in tension along build direction is considered in the formulation. The optimized design is shown in Figure 6b.

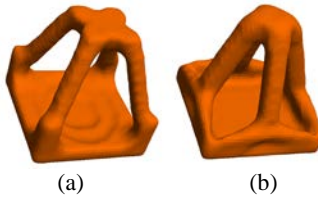


**Figure 6:** Tensile stool. Optimized design with respect to (a) Stiffness (b) Strength and weak in Z.

Figure 7 illustrates the change in  $\gamma$  throughout the optimization process for the second experiment. Observe that since the objective function is not self-adjoint, the Pareto front is also not convex.

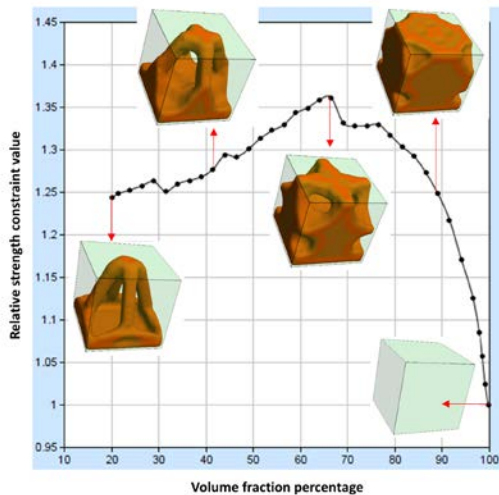


**Figure 7:** Tensile stool. Optimization process.

**Experimental Validation.** To validate the numerical results, the designs of Figure 6 were printed and tested. An XYZ Da Vinci Duo was used to print four samples for each example. Samples were printed at 90% infill density (maximum allowable

percentage by the software) with 2 shell layers. It is important to note that the build direction for all samples is the vertical direction and raster orientation is  $\pm 45^\circ$ . The same generic brand of ABS was used to print the specimens. Tests were conducted using an MTS Criterion Model 43 system with 5 kN load cell. Built in LVDTs measured the displacement between the grips. Displacement control tests were run at 5 mm/min with data collection rate of 100 Hz. Load and displacement were recorded for further analysis. Figure 9 illustrates the tensile test setup on an MTS criterion model 43 tensile actuator.



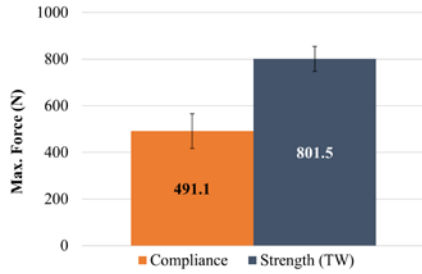
**Figure 8:** Tensile stool: tensile test setup for optimized stool designs.

Figure 9 illustrates the failed parts, observe that failure plane is perpendicular to the build direction.



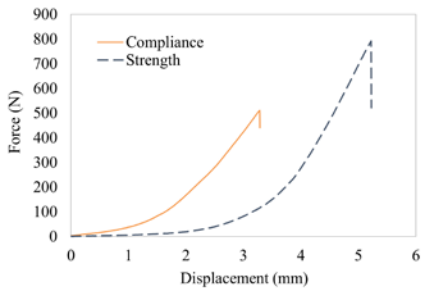
**Figure 9:** Tensile stool: tensile test, considering (left) anisotropic strengths and (right) stiffness.

Figure 10 summarizes the tensile test results. Four samples were tested per design. The design optimized for stiffness on average endured force of about 491 N, while this was improved to 801 N for the optimized design considering strength and anisotropic behavior along build direction.



**Figure 10:** Tensile stool. Tensile test results.

Figure 11 illustrates the force-displacement graph of both tensile tests. Observe that the design optimized for strength has higher load capacity. Further, it is worth noting that both tests indicate brittle fracture, which in future needs to be incorporated optimization process.



**Figure 11:** Tensile stool. Typical force-displacement graph.

## 4.2 Tension Versus Compression

In this experiment, we demonstrate that the proposed method captures the difference between tension and compression loading. Consider the C-bracket of Figure 12, where the bottom left surface is fixed. The domain is discretized into 20,000 hexahedral elements. In examples of Figure 12a and Figure 12b a downward and an upward force is acting at the right tip, causing the fillet to be under compression and tension, respectively. The objective is to find the strongest design while removing 50% of the material.

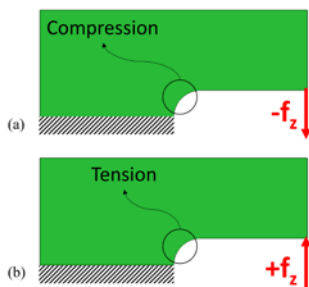


**Figure 12:** C-Bracket. Geometry and loading for a) Compression at fillet and b) Tension at fillet.

To compare the results, we first find the strongest design based on vonMises criterion [48], for which the result is shown in Figure 13a. Note that since vonMises does not capture directional preference, for both load cases the optimized design is the same.

Observe that in the case of downward load, vonMises criterion fails to identify the actual failure region verified through experiment.

Next, the Tsai-Wu criterion was used to find the optimal topologies. Figure 13b illustrates the optimized design when the fillet is under compression. The optimized design is similar to that of Figure 13a with isotropic strengths. However, Tsai-Wu criterion successfully identifies the actual region of failure.

Figure 13c illustrates the optimized design when the fillet is under tension. Observe that in order to reduce stress concentration, the proposed optimizer increases the fillet radius. Moreover, Tsai-Wu criterion successfully identifies the actual failure point.

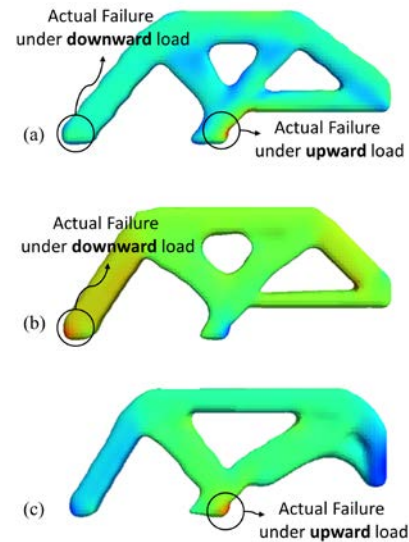


**Figure 13:** C-Bracket. Optimized designs with underlying stress field.

a) Isotropic strength with vonMises field b) Weak Z compression at fillet with Tsai-Wu field and c) Weak Z tension at fillet with Tsai-Wu field.

**Experimental Validation.** To compare the performance of optimized designs under loadings of Figure 12a and Figure 12b, each design was printed using the same printer with the same printing parameters as mentioned before. The sample size is four for each design. A custom test fixture was designed to accommodate both tests in tension and compression. Testing parameters were also kept the same for the C-Bracket in both set of tests.

Figure 14 shows the test setup for exerting downward force and causing compression at fillet. Figure 15 shows the bending test results for C-bracket under compression. Results show a statistically equal strength for both designs. This conclusion agrees with von Mises and Tsai-Wu criteria predictions.



Figure 14: C-Bracket Fillet under compression. Test setup.



Figure 15: C-Bracket: fillet under compression.

On the other hand, results for bending test when C-bracket is under tension (Figure 16) favors heavily towards the design from Tsai-Wu criterion with an average maximum force of 116.1 N compared with maximum average force of 69.3 N (Figure 17).



Figure 16: C-Bracket Fillet under Tension. Test setup.

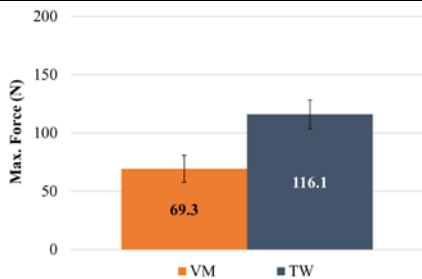


Figure 17: C-Bracket. Fillet under Tension.

It is also worth noting that the design of Figure 13a, which is optimized via vonMises criterion, is about 4.7 times stronger

under compressive load than tensile load. Since the failure plane is perpendicular to build direction, this is in agreement with the notion that FDM printed designs are much weaker in tension than compression along build direction.

## 5. Summary and Future Work

In this paper, we have proposed a method to compute strength sensitivity based on generalized failure criteria such as Tsai-Wu for anisotropic parts. For numerical experiments, we have focused on anisotropic strengths of additively manufactured parts where tensile strength along build direction is lower than other directions. Table 2 summarizes the results for the numerical examples.

Table 2: Summary of Experiments (VM: vonMises, TW: Tsai-Wu)

Example	#DOF	Time(s) VM/TW	Rel. J VM/TW	Rel. Obj. VM/TW
Tensile stool	164,616	235/260	2.28/2.57	0.99/1.60
C-Bracket (compression)	68,661	41/42	1.62/1.56	1.17/1.22
C-Bracket (tension)	68,661	41/50	1.76/1.56	1.12/1.22

The proposed framework can be extended to also include constitutive anisotropy, which requires accurate tensile and shear measurements. Also, the fact that the materials is brittle must be taken into consideration through a more comprehensive fracture model and sensitivity analysis. Moreover, the current printing processes introduce uncertainty in the material behavior, considering robustness can also be beneficial. Furthermore, the sensitivity can be extended to strength-based multi-material topology optimization. For multiple materials, since each material has its own strength, vonMises criterion is inadequate and more generalized failure indices are suitable. However, local de-bonding effects must also be considered.

## Acknowledgements

The authors would like to thank the support of National Science Foundation through grants CMMI-1561899, IIP-1500205, through grants CMMI-1232508, CMMI-1161474, and DOE through ARPA-E ARID grant. Prof. Krishnan is a CEO of SciArt, LLC, which has licensed the Pareto technology reported in this publication, through Wisconsin Alumni Research Foundation.

## Appendix

Consider the definition in Equation (23). Exploiting the p-norm definition in Equation (12), we have:

$$\mathbf{g} = \frac{1}{p} \left( \sum_e (\gamma_e)^p \right)^{1/p-1} \left( \sum_e p (\gamma_e)^{p-1} \frac{\partial \gamma_e}{\partial \mathbf{u}} \right) \quad (29)$$

must solve the following adjoint problem [65],

$$\mathbf{K}\boldsymbol{\mu} = \mathbf{g}^T \quad (30)$$

where  $\boldsymbol{\mu}$  is the adjoint solution and  $\mathbf{g}^T$  is the adjoint force.

We are assuming hexahedral elements (with 8 nodes). Recalling Equations (5) and (10), the inverse of the strength ratio at each

element  $\gamma_e$  depends on individual stress components at that element, which are evaluated as follows:

$$\{\sigma\}_{(6,1)} = [D]_{(6,6)} [B]_{(6,24)} \{u\}_{(24,1)} \quad (31)$$

where  $[D]$  is material tensor,  $[B]$  is the gradient matrix, and

$$\begin{aligned} \{\sigma\}_{(6,1)} &= \{\sigma_{11} \quad \sigma_{22} \quad \sigma_{33} \quad \sigma_{23} \quad \sigma_{31} \quad \sigma_{12}\}^T \\ \{u\}_{(24,1)} &= \{u_1 \quad v_1 \quad w_1 \quad \dots \quad u_8 \quad v_8 \quad w_8\} \end{aligned} \quad (32)$$

Hence, in order to evaluate Equation (23) we must evaluate Equation (34):

$$\frac{\partial \gamma_e}{\partial \mathbf{u}} = \left[ \frac{2 \frac{d\mathcal{A}}{d\mathbf{u}}}{\left(-\mathcal{B} + \sqrt{\mathcal{B}^2 + 4\mathcal{A}}\right)} - 2\mathcal{A} \left( \frac{d\mathcal{B}}{d\mathbf{u}} + \frac{2\mathcal{B} \frac{d\mathcal{B}}{d\mathbf{u}} + 4 \frac{d\mathcal{A}}{d\mathbf{u}}}{\sqrt{\mathcal{B}^2 + 4\mathcal{A}}} \right) \right] \frac{1}{\left(-\mathcal{B} + \sqrt{\mathcal{B}^2 + 4\mathcal{A}}\right)^2} \quad (33)$$

where  $\mathcal{A}$  and  $\mathcal{B}$  are defined in Equation (5) and their derivatives are the generalization of the equations in [48],

$$\frac{d\mathcal{A}}{d\mathbf{u}} = 2 \begin{bmatrix} C_{12} (F_{1,:} \sigma_{22} + F_{2,:} \sigma_{11}) + C_{13} (F_{1,:} \sigma_{33} + F_{3,:} \sigma_{11}) \\ + C_{23} (F_{2,:} \sigma_{33} + F_{3,:} \sigma_{22}) \\ + C_{11} (F_{1,:} \sigma_{11}) + C_{22} (F_{2,:} \sigma_{22}) + C_{33} (F_{3,:} \sigma_{33}) \\ + C_{44} (F_{4,:} \sigma_{23}) + C_{55} (F_{5,:} \sigma_{31}) + C_{66} (F_{6,:} \sigma_{12}) \end{bmatrix} \quad (34)$$

$$\frac{d\mathcal{B}}{d\mathbf{u}} = C_1 F_{1,:} + C_2 F_{2,:} + C_3 F_{3,:} \quad (35)$$

and

$$[F]_{(6,24)} = [D]_{(6,6)} [B]_{(6,24)} \quad (36)$$

It is worth noting that in Equation (30), material anisotropy affects both stiffness matrix  $\mathbf{K}$  through material tensor  $\mathbf{D}$  and adjoint force  $\mathbf{g}^T$  (through Tsai-Wu coefficients  $C_{ij}$   $i, j = 1, \dots, 6$ ).

## References

[1] S. S. Babu, L. Love, R. Dehoff, W. Peter, T. R. Watkins, and S. Pannala, "Additive manufacturing of materials: Opportunities and challenges," *MRS Bulletin*, vol. 40, no. 12, pp. 1154–1161, Dec. 2015.

[2] B. Khoshnevis, D. Hwang, K.-T. Yao, and Z. Yeh, "Mega-scale fabrication by Contour Crafting," *International Journal of Industrial and Systems Engineering*, vol. 1, no. 3, pp. 301–320, Jan. 2006.

[3] A. Bandyopadhyay, S. Bose, and S. Das, "3D printing of biomaterials," *MRS Bulletin*, vol. 40, no. 2, pp. 108–115, Feb. 2015.

[4] "Case Studies," *Voxel8*. [Online]. Available: <http://www.voxel8.com/case-studies/>. [Accessed: 21-Nov-2016].

[5] R. P. Hoyt, "SpiderFab: An Architecture for Self-Fabricating Space Systems," in *AIAA SPACE 2013 Conference and Exposition*, American Institute of Aeronautics and Astronautics.

[6] O. Sigmund, "A 99 line topology optimization code written in Matlab," *Structural and Multidisciplinary Optimization*, vol. 21, no. 2, pp. 120–127, 2001.

[7] G. Allaire, F. Jouve, and A.-M. Toader, "A level-set method for shape optimization," *Comptes Rendus Mathematique*, vol. 334, no. 12, pp. 1125–1130, 2002.

[8] K. Suresh, "A 199-line Matlab code for Pareto-optimal tracing in topology optimization," *Struct Multidisc Optim*, vol. 42, no. 5, pp. 665–679, Nov. 2010.

[9] D. Brackett, I. Ashcroft, and R. Hague, "Topology optimization for additive manufacturing," in *22nd Annual international solid freeform fabrication symposium*, 2011, pp. 348–362.

[10] J. C. Riddick, M. A. Haile, R. V. Wahlde, D. P. Cole, O. Bamiduro, and T. E. Johnson, "Fractographic analysis of tensile failure of acrylonitrile-butadiene-styrene fabricated by fused deposition modeling," *Additive Manufacturing*, vol. 11, pp. 49–59, Jul. 2016.

[11] B. Rankouhi, S. Javadpour, F. Delfanian, and T. Letcher, "Failure Analysis and Mechanical Characterization of 3D Printed ABS With Respect to Layer Thickness and Orientation," *J Fail. Anal. and Preven.*, vol. 16, no. 3, pp. 467–481, Jun. 2016.

[12] A. A. Novotny, R. A. Feijóo, E. Taroco, and C. Padra, "Topological sensitivity analysis for three-dimensional linear elasticity problem," *Computer Methods in Applied Mechanics and Engineering*, vol. 196, no. 41, pp. 4354–4364, 2007.

[13] N. E. Dowling, *Mechanical behavior of materials : engineering methods for deformation, fracture, and fatigue*. Prentice Hall, 1993.

[14] O. Pironneau, "Optimal shape design for elliptic systems," in *System Modeling and Optimization*, R. F. Drenick and F. Kozin, Eds. Springer Berlin Heidelberg, 1982, pp. 42–66.

[15] J. Sokolowski and J.-P. Zolesio, "Introduction to shape optimization," in *Introduction to Shape Optimization*, Springer Berlin Heidelberg, 1992, pp. 5–12.

[16] X. Changwen and Y. Minghua, "Shape optimization of structures to minimize stress concentration," *Computers & Structures*, vol. 36, no. 3, pp. 491–497, 1990.

[17] G. Sved and Z. Ginos, "Structural optimization under multiple loading," *International Journal of Mechanical Sciences*, vol. 10, no. 10, pp. 803–805, Oct. 1968.

[18] U. KIRSCH, "Optimal Topologies of Flexural Systems," *Engineering Optimization*, vol. 11, no. 1–2, pp. 141–149, Apr. 1987.

[19] U. Kirsch, "On singular topologies in optimum structural design," *Structural Optimization*, vol. 2, no. 3, pp. 133–142, Sep. 1990.

[20] G. Xu and C. Gengdong, "Epsilon-continuation approach for truss topology optimization," *Acta Mech Sinica*, vol. 20, no. 5, pp. 526–533, Oct. 2004.

- [21] G. Cheng and Z. Jiang, "Study on Topology Optimization with Stress Constraints," *Engineering Optimization*, vol. 20, no. 2, pp. 129–148, Nov. 1992.
- [22] G. D. Cheng and X. Guo, "ε-relaxed approach in structural topology optimization," *Structural Optimization*, vol. 13, no. 4, pp. 258–266, Jun. 1997.
- [23] P. Duysinx, L. Van Miegroet, E. Lemaire, O. Bruls, and M. Bruyneel, "Topology and generalized shape optimization: Why stress constraints are so important?," *International Journal for Simulation and Multidisciplinary Design Optimization*, vol. 2, no. 4, pp. 253–258, Dec. 2008.
- [24] G. I. N. Rozvany, "On design-dependent constraints and singular topologies," *Struct Multidisc Optim*, vol. 21, no. 2, pp. 164–172, Feb. 2014.
- [25] M. P. Bendse and N. Kikuchi, "Generating optimal topologies in structural design using a homogenization method," *Computer Methods in Applied Mechanics and Engineering*, vol. 71, no. 2, pp. 197–224, Nov. 1988.
- [26] M. P. Bendse, "Optimal shape design as a material distribution problem," *Structural Optimization*, vol. 1, no. 4, pp. 193–202, Dec. 1989.
- [27] Y. M. Xie and G. P. Steven, "A simple evolutionary procedure for structural optimization," *Computers & Structures*, vol. 49, no. 5, pp. 885–896, Dec. 1993.
- [28] M. Zhou and G. I. N. Rozvany, "On the validity of ESO type methods in topology optimization," *Struct Multidisc Optim*, vol. 21, no. 1, pp. 80–83, Mar. 2001.
- [29] R. J. Yang and C. J. Chen, "Stress-based topology optimization," *Structural Optimization*, vol. 12, no. 2–3, pp. 98–105, Oct. 1996.
- [30] P. Duysinx and M. P. Bendse, "Topology optimization of continuum structures with local stress constraints," *Int. J. Numer. Meth. Engng.*, vol. 43, no. 8, pp. 1453–1478, Dec. 1998.
- [31] M. Bruggi and P. Venini, "A mixed FEM approach to stress-constrained topology optimization," *Int. J. Numer. Meth. Engng.*, vol. 73, no. 12, pp. 1693–1714, Mar. 2008.
- [32] M. Bruggi, "On an alternative approach to stress constraints relaxation in topology optimization," *Struct Multidisc Optim*, vol. 36, no. 2, pp. 125–141, Jan. 2008.
- [33] C. Le, J. Norato, T. Bruns, C. Ha, and D. Tortorelli, "Stress-based topology optimization for continua," *Struct Multidisc Optim*, vol. 41, no. 4, pp. 605–620, Oct. 2009.
- [34] J. Pars, F. Navarrina, I. Colominas, and M. Casteleiro, "Topology optimization of continuum structures with local and global stress constraints," *Struct Multidisc Optim*, vol. 39, no. 4, pp. 419–437, Nov. 2008.
- [35] J. Pars, F. Navarrina, I. Colominas, and M. Casteleiro, "Stress constraints sensitivity analysis in structural topology optimization," *Computer Methods in Applied Mechanics and Engineering*, vol. 199, no. 33–36, pp. 2110–2122, Jul. 2010.
- [36] E. Holmberg, B. Torstenfelt, and A. Klarbring, "Stress constrained topology optimization," *Struct Multidisc Optim*, vol. 48, no. 1, pp. 33–47, Feb. 2013.
- [37] J. A. Sethian, "A fast marching level set method for monotonically advancing fronts," *PNAS*, vol. 93, no. 4, pp. 1591–1595, Feb. 1996.
- [38] J. A. Sethian, *Level Set Methods and Fast Marching Methods: Evolving Interfaces in Computational Geometry, Fluid Mechanics, Computer Vision, and Materials Science*. Cambridge University Press, 1999.
- [39] L. V. Miegroet and P. Duysinx, "Stress concentration minimization of 2D fillets using X-FEM and level set description," *Struct Multidisc Optim*, vol. 33, no. 4–5, pp. 425–438, Jan. 2007.
- [40] K. Svanberg and M. Werme, "Sequential integer programming methods for stress constrained topology optimization," *Struct Multidisc Optim*, vol. 34, no. 4, pp. 277–299, May 2007.
- [41] G. Allaire and F. Jouve, "Minimum stress optimal design with the level set method," *Engineering Analysis with Boundary Elements*, vol. 32, no. 11, pp. 909–918, Nov. 2008.
- [42] M. Yulin and W. Xiaoming, "A level set method for structural topology optimization and its applications," *Advances in Engineering Software*, vol. 35, no. 7, pp. 415–441, Jul. 2004.
- [43] J. A. Norato, M. P. Bendse, R. B. Haber, and D. A. Tortorelli, "A topological derivative method for topology optimization," *Struct Multidisc Optim*, vol. 33, no. 4–5, pp. 375–386, Apr. 2007.
- [44] G. Allaire, F. De Gournay, F. Jouve, and A. Toader, "Structural optimization using topological and shape sensitivity via a level set method," *Control and cybernetics*, vol. 34, no. 1, p. 59, 2005.
- [45] S. Amstutz and A. A. Novotny, "Topological optimization of structures subject to Von Mises stress constraints," *Struct Multidisc Optim*, vol. 41, no. 3, pp. 407–420, Aug. 2009.
- [46] Q. Xia, T. Shi, S. Liu, and M. Y. Wang, "A level set solution to the stress-based structural shape and topology optimization," *Computers & Structures*, vol. 90–91, pp. 55–64, Jan. 2012.
- [47] N. M. K. Poon and J. R. R. A. Martins, "An adaptive approach to constraint aggregation using adjoint sensitivity analysis," *Struct Multidisc Optim*, vol. 34, no. 1, pp. 61–73, Dec. 2006.
- [48] K. Suresh and M. Takaloozadeh, "Stress-constrained topology optimization: a topological level-set approach," *Struct Multidisc Optim*, vol. 48, no. 2, pp. 295–309, Mar. 2013.
- [49] S. Cai, W. Zhang, J. Zhu, and T. Gao, "Stress constrained shape and topology optimization with fixed mesh: A B-spline finite cell method combined with level set function," *Computer Methods in Applied Mechanics and Engineering*, vol. 278, pp. 361–387, Aug. 2014.
- [50] H. Emmendoerfer and E. A. Fancello, "A level set approach for topology optimization with local stress constraints," *Int. J. Numer. Meth. Engng*, vol. 99, no. 2, pp. 129–156, Jul. 2014.
- [51] S. Cai and W. Zhang, "Stress constrained topology optimization with free-form design domains," *Computer Methods in Applied Mechanics and Engineering*, vol. 289, pp. 267–290, Jun. 2015.
- [52] M. Schneider and H. Andr, "The topological gradient in anisotropic elasticity with an eye towards lightweight

- design,” *Mathematical Methods in the Applied Sciences*, vol. 37, no. 11, pp. 1624–1641, Jul. 2014.
- [53] G. Delgado and M. Bonnet, “The topological derivative of stress-based cost functionals in anisotropic elasticity,” *Computers & Mathematics with Applications*, vol. 69, no. 10, pp. 1144–1166, May 2015.
- [54] R. Hill, *The Mathematical Theory of Plasticity*. Clarendon Press, 1998.
- [55] V. D. Azzi and S. W. Tsai, “Anisotropic strength of composites,” *Experimental Mechanics*, vol. 5, no. 9, pp. 283–288, Sep. 1965.
- [56] O. Hoffman, “The Brittle Strength of Orthotropic Materials,” *Journal of Composite Materials*, vol. 1, no. 2, pp. 200–206, Apr. 1967.
- [57] S. W. Tsai and E. M. Wu, “A General Theory of Strength for Anisotropic Materials,” *Journal of Composite Materials*, vol. 5, no. 1, pp. 58–80, Jan. 1971.
- [58] J.-M. Berthelot, *Composite Materials: Mechanical Behavior and Structural Analysis*. Springer Science & Business Media, 1999.
- [59] A. A. Groenwold and R. T. Haftka, “Optimization with non-homogeneous failure criteria like Tsai–Wu for composite laminates,” *Struct Multidisc Optim*, vol. 32, no. 3, pp. 183–190, Jul. 2006.
- [60] G. Y. Qiu and X. S. Li, “A note on the derivation of global stress constraints,” *Struct Multidisc Optim*, vol. 40, no. 1–6, p. 625, May 2009.
- [61] X. Guo, W. S. Zhang, M. Y. Wang, and P. Wei, “Stress-related topology optimization via level set approach,” *Computer Methods in Applied Mechanics and Engineering*, vol. 200, no. 47–48, pp. 3439–3452, Nov. 2011.
- [62] J. Nocedal and S. Wright, *Numerical Optimization*. Springer Science & Business Media, 2006.
- [63] S. Deng and K. Suresh, “Multi-constrained topology optimization via the topological sensitivity,” *Struct Multidisc Optim*, vol. 51, no. 5, pp. 987–1001, Nov. 2014.
- [64] R. A. Feijoo, A. A. Novotny, E. Taroco, and C. Padra, “The topological-shape sensitivity method in two-dimensional linear elasticity topology design,” *Applications of Computational Mechanics in Structures and Fluids*, 2005.
- [65] A. M. Mirzendehtdel and K. Suresh, “A Pareto-Optimal Approach to Multimaterial Topology Optimization,” *J. Mech. Des*, vol. 137, no. 10, pp. 101701–101701, Aug. 2015.
- [66] K. Suresh, “Efficient generation of large-scale pareto-optimal topologies,” *Struct Multidisc Optim*, vol. 47, no. 1, pp. 49–61, May 2012.
- [67] Sung-Hoon Ahn, Michael Montero, Dan Odell, Shad Roundy, and Paul K. Wright, “Anisotropic material properties of fused deposition modeling ABS,” *Rapid Prototyping Journal*, vol. 8, no. 4, pp. 248–257, Oct. 2002.
- [68] Sung Hoon Ahn, Changil Baek, Sunyoung Lee, and In Shup Ahn, “Anisotropic Tensile Failure Model of Rapid Prototyping Parts - Fused Deposition Modeling (FDM),” *Int. J. Mod. Phys. B*, vol. 17, no. 08n09, pp. 1510–1516, Apr. 2003.